Charge carrier drift in SolidStateDetectors.jl

1 Parameterisation of the longitudinal charge carrier drift

The charge carrier drift in solid state materials is influenced by the crystal symmetry. A face-centred cubic crystal lattice is invariant under rotations around any of the three main crystal axes, $\langle 100 \rangle$, $\langle 110 \rangle$ and $\langle 111 \rangle$. If the electric field points along one of these axes, also the drift velocity needs to be invariant under these rotations. Hence, the longitudinal drift velocity for electrons and holes, $\upsilon_{e/h}$, drifting along the crystal axes needs to be aligned with the electric field and is

$$\upsilon_{e/h} = \mu_{e/h} E, \tag{1}$$

where $E = |\vec{E}|$ is the electric field strength and $\mu_{e/h}$ denotes the electron or hole mobility, respectively. On the crystal axes and for small E, μ_e and μ_h are scalar constants.

However, for $E \gtrsim 100\,\mathrm{V/cm}$, the drift velocity does not anymore increase linearly with the electric field strength and approaches a saturation value. A phenomenological parameterisation to model the drift velocity was introduced by D.M. Caughey *et al.* [1] which was later expanded by adding a negative term by L. Mihailescu *et al.* [2]:

$$\upsilon_{e/h} = \frac{\mu_0 E}{(1+(E/E_0)^{\beta})^{1/\beta}} - \mu_n E. \tag{2}$$

Both, β and E_0 are temperature-dependent parameters obtainable from measurements on electrons and holes along each of the crystal axes, respectively. The term with the parameter μ_n accounts for the Gunn effect [3] and is only relevant for electrons.

For germanium, the parameters for Eq. (2) as extracted by fits to experimental data [4] were measured at a reference temperature of $T_0 = 78\,\mathrm{K}$, see Tab. 1. While for each charge carrier type, the drift mobility μ_0 does not differ much along the different directions, the parameter β varies significantly. For electric fields $E \ll E_0$, this results in $\upsilon \approx \mu_0 E$ which describes an isotropic movement of the charge carriers along all directions, $\upsilon^{100} = \upsilon^{110} = \upsilon^{111}$. However, for high electric fields with $E \gtrsim E_0$, the charge carrier drift becomes anisotropic, $\upsilon^{100} > \upsilon^{110} > \upsilon^{111}$ [5]. This anisotropy is important for normal detector operation.

Table 1: Literature values for the drift velocity parameters in Eq. (2) for electrons and holes along the $\langle 100 \rangle$ and $\langle 111 \rangle$-direction in germanium at $T_0 = 78\,\mathrm{K}$, taken from [4].

Charge carrier	Direction	μ_0 in $\frac{\mathrm{cm}^2}{\mathrm{Vs}}$	E_0 in $\frac{\mathrm{V}}{\mathrm{cm}}$	β	μ_n in $\frac{\mathrm{cm}^2}{\mathrm{Vs}}$
Electrons	$\langle 100 \rangle$	38609	511	0.805	-171
	$\langle 111 \rangle$	38536	538	0.641	510
Holes	$\langle 100 \rangle$	61824	185	0.942	
	$\langle 111 \rangle$	61215	182	0.662	

2 Electron drift model as implemented in SolidStateDetectors.jl

If at a given position, $\vec{r}$, the electric field $\vec{E}(\vec{r})$ is not aligned with any of the crystal axes, the electron drift velocity, $\vec{\upsilon}_e$, does not necessarily need to follow $\vec{E}$. Hence, the electron mobility, μ_e, needs to be described as a tensor:

$$\vec{\upsilon}_e(\vec{r}) = \mu_e(\vec{E}(\vec{r}))\,\vec{E}(\vec{r}). \tag{3}$$

Note that the $\langle 100\rangle$, $\langle 110\rangle$ and $\langle 111\rangle$-directions need to be eigenvectors of μ_e with eigenvalues satisfying Eq. (2).

There are several approaches how to theoretically model $\vec{\upsilon}_e$ in germanium. In the drift model studied by L. Mihailescu *et al.* [2], the electron drift velocity is described by

$$\vec{\upsilon}_e(\vec{r}) = \underbrace{\mathscr{A}(E(\vec{r}))\sum_j \frac{n_j}{n}\frac{\gamma_j}{\sqrt{\vec{E}^\dagger(\vec{r})\gamma_j\vec{E}(\vec{r})}}}_{=\mu_e(\vec{E}(\vec{r}))}\vec{E}(\vec{r}), \tag{4}$$

where only electrons in the four conduction band minima at the L-points are considered. Here, $\mathscr{A}$ is an empirical function which absorbs the dependence on E, γ_j is the tensor of reciprocal effective electron masses and $\frac{n_j}{n}$ is the fraction of electrons in the j-th valley. Equation (4) effectively averages the contributions of each conduction band minimum to the total drift velocity, weighted by the fraction of electrons which populate the respective minimum.

The charge carrier fraction in the j-th conduction band minimum can be expressed [2] by introducing an empirical function, $\mathscr{R}$, which scales the deviation from an equal distribution, $\frac{n_e}{n}$. The approach from H.G. Reik and H. Risken [6] results in

$$\frac{n_j}{n} = \mathscr{R}(E(\vec{r}))\left(\frac{(\vec{E}^\dagger(\vec{r})\gamma_j\vec{E}(\vec{r}))^{-1/2}}{\sum_i(\vec{E}^\dagger(\vec{r})\gamma_i\vec{E}(\vec{r}))^{-1/2}} - \frac{n_e}{n}\right) + \frac{n_e}{n}. \tag{5}$$

If the electric field points along the $\langle 100\rangle$ axis, all four conduction band minima are equally populated, i.e. $\frac{n_j}{n} = \frac{n_e}{n}$, and contribute equally to $\vec{\upsilon}_e$ [7]. For other electric field orientations, the assumption of an equal distribution does not necessarily hold.

The functions $\mathscr{A}$ and $\mathscr{R}$ completely define the response of $\vec{\upsilon}_e$ to an electric field $\vec{E}$. Thus, the determination of these functions are described in detail for germanium and silicon within the following subsections.

2.1 Germanium

In germanium, only the electrons in the four degenerate conduction band minima at the L-points of the first Brillouin zone are taken into account. The effective masses of the electrons in these valleys depend on the direction of the electric field and take values between the transverse effective electron mass, $m^*_{e,T}$, and the longitudinal effective electron mass, $m^*_{e,L}$. In units of the electron mass, $m^*_{e,T} = 0.0819$ and $m^*_{e,L} = 1.64$ [8].

2.1.1 Determination of γ_j

For each conduction band minimum j, γ_j can be obtained by transforming the reciprocal effective mass tensor

$$\gamma_0 = \begin{pmatrix} 1/m^*_{e,T} & 0 & 0 \\ 0 & 1/m^*_{e,L} & 0 \\ 0 & 0 & 1/m^*_{e,T} \end{pmatrix}$$

from the local coordinate system $x'y'z'$ of the conduction band minima, with the initial y'-axis pointing towards the $\langle 111 \rangle$-direction, to a global xyz coordinate system, see Fig. 1. The transformation consists of two rotations: one rotation by $\mathrm{acos}(\sqrt{2/3})$ around the x'-axis to align the y'-axis with the $\langle 110 \rangle$ axis and one rotation by φ_{110} around the z-axis to align the y'-axis with the y-axis. Mathematically, the rotations are expressed through rotation matrices

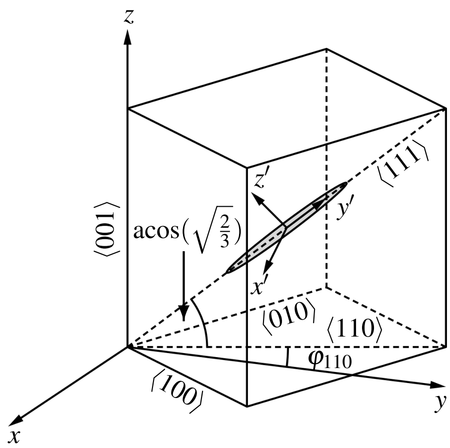

Figure 1: Relation between the local coordinates $x'y'z'$ in the conduction band minima and the crystal coordinate system xyz. The y'-axis in the local coordinate system is aligned with the $\langle 111 \rangle$ axis.

$$R_j = R_{x'}(\mathrm{acos}(\sqrt{2/3}))\, R_z(\varphi_{110} + j\pi/2),$$

resulting in reciprocal effective mass tensors of $\gamma_j = R_j^{-1} \gamma_0 R_j$. Using the abbreviations $T = 1/m^*_{e,T}$, $L = 1/m^*_{e,L}$, $c_j = \cos(\varphi_{110} + j\pi/2)$ and $s_j = \sin(\varphi_{110} + j\pi/2)$ yields

$$\begin{aligned}
\gamma_j = R_j^{-1}\gamma_0 R_j &= R_z^{-1}(\varphi_{110} + j\pi/2)\, R_{x'}^{-1}(\mathrm{acos}(\sqrt{2/3}))\, \gamma_0\, R_{x'}(\mathrm{acos}(\sqrt{2/3}))\, R_z(\varphi_{110} + j\pi/2) \\
&= \begin{bmatrix} c_j & -s_j & 0 \\ s_j & c_j & 0 \\ 0 & 0 & 1 \end{bmatrix}
\begin{bmatrix} 1 & 0 & 0 \\ 0 & \sqrt{\frac{2}{3}} & -\sqrt{\frac{1}{3}} \\ 0 & \sqrt{\frac{1}{3}} & \sqrt{\frac{2}{3}} \end{bmatrix}
\begin{bmatrix} T & 0 & 0 \\ 0 & L & 0 \\ 0 & 0 & T \end{bmatrix}
\begin{bmatrix} 1 & 0 & 0 \\ 0 & \sqrt{\frac{2}{3}} & \sqrt{\frac{1}{3}} \\ 0 & -\sqrt{\frac{1}{3}} & \sqrt{\frac{2}{3}} \end{bmatrix}
\begin{bmatrix} c_j & s_j & 0 \\ -s_j & c_j & 0 \\ 0 & 0 & 1 \end{bmatrix} \\
&= \begin{bmatrix} T + \frac{2}{3}s_j^2(L-T) & -\frac{2}{3}c_j s_j(L-T) & -\frac{\sqrt{2}}{3}s_j(L-T) \\ -\frac{2}{3}c_j s_j(L-T) & T + \frac{2}{3}c_j^2(L-T) & \frac{\sqrt{2}}{3}c_j(L-T) \\ -\frac{\sqrt{2}}{3}s_j(L-T) & \frac{\sqrt{2}}{3}c_j(L-T) & \frac{2}{3}T + \frac{1}{3}L \end{bmatrix},
\end{aligned} \tag{6}$$

where the j-dependence is found in the expressions for c_j and s_j.

To derive analytical expressions for the empirical functions $\mathscr{A}$ and $\mathscr{R}$, the y-axis in the global coordinate system is chosen such that it is aligned with the $\langle 110 \rangle$ axis, i.e. $\varphi_{110} = 0$. However, the choice of φ_{110} does not influence the results for $\mathscr{A}$ or $\mathscr{R}$.

2.1.2 Determination of $\mathscr{A}$

When setting $\varphi_{110} = 0$, the direction of an electric field, $\vec{E}_0 = \vec{E}/|\vec{E}|$, along the $\langle 100 \rangle$ axis is given by $\vec{E}_0 = [\sqrt{1/2}, \sqrt{1/2}, 0]$. Together with Eq. (6), the term in the denominator in Eq. (4) for all conduction band minima, j, takes the form

$$\vec{E}_0^\dagger \gamma_j \vec{E}_0 = \frac{2}{3}T + \frac{1}{3}L$$

which does not depend on j. As no minimum is favoured over the others, all conduction band minima are equally populated, i.e. $\frac{n_j}{n} = \frac{1}{4}$. This results in

$$\vec{v}_e(E) = \mathscr{A}(E) \sum_{j=1}^{4} \frac{n_j}{n} \frac{\gamma_j \vec{E}_0}{\sqrt{\vec{E}_0^\dagger \gamma_j \vec{E}_0}} = \mathscr{A}(E) \frac{1}{4} \frac{1}{\sqrt{\frac{2}{3}T + \frac{1}{3}L}} \sum_{j=1}^{4} \gamma_j \vec{E}_0 \, .$$

Using $\sum_{j=1}^4 s_j = \sum_{j=1}^4 c_j = \sum_{j=1}^4 c_j s_j = 0$ and $\sum_{j=1}^4 s_j^2 = \sum_{j=1}^4 c_j^2 = 2$ yields

$$\sum_{j=1}^{4} \gamma_j = \begin{bmatrix} \frac{8}{3}T + \frac{4}{3}L & 0 & 0 \\ 0 & \frac{8}{3}T + \frac{4}{3}L & 0 \\ 0 & 0 & \frac{8}{3}T + \frac{4}{3}L \end{bmatrix} \mathrel{\hat{=}} \frac{8}{3}T + \frac{4}{3}L$$

Along the $\langle 100 \rangle$ axis, $\vec{v}_e$ and $\vec{E}_0$ are expected to be aligned, i.e. $\vec{v}_e(E) = v_e^{100}(E)\,\vec{E}_0$.

$$\begin{aligned} \Rightarrow \vec{v}_e(E) &= \mathscr{A}(E) \frac{1}{4} \frac{1}{\sqrt{\frac{2}{3}T + \frac{1}{3}L}} \left(\frac{8}{3}T + \frac{4}{3}L \right) \vec{E}_0 \\ \vec{v}_e(E) &= \mathscr{A}(E) \sqrt{\frac{2}{3}T + \frac{1}{3}L}\, \vec{E}_0 \stackrel{!}{=} v_e^{100}(E)\,\vec{E}_0 \\ \Rightarrow \mathscr{A}(E) &= \frac{v_e^{100}(E)}{\sqrt{\frac{2}{3}T + \frac{1}{3}L}} =: \frac{v_e^{100}(E)}{\Gamma_0}, \end{aligned} \tag{7}$$

where $\Gamma_0 = \sqrt{\frac{2}{3}T + \frac{1}{3}L}$. Using $m^*_{e,T} = 0.0819$ and $m^*_{e,L} = 1.64$ results in $\Gamma_0 = 2.888$.

2.1.3 Determination of $\mathscr{R}$

If $\varphi_{110} = 0$, an electric field along the $\langle 111 \rangle$ axis is given by $\vec{E}_0 = [\sqrt{2/3}, 0, \sqrt{1/3}]$. Here, $\vec{E}_0^\dagger \gamma_j \vec{E}_0$ depends on j. One of the minima, $j = 1$, is aligned with the electric field, giving $\vec{E}_0^\dagger \gamma_1 \vec{E}_0 = L$, while the other three, $j = 2,3,4$, yield $\vec{E}_0^\dagger \gamma_j \vec{E}_0 = \frac{8}{9}T + \frac{1}{9}L$. This leads to the fact that one charge carrier fraction, i.e. $\frac{n_1}{n}$, is different from the other three, $\frac{n_2}{n} = \frac{n_3}{n} = \frac{n_4}{n}$. Inserting the values for $\gamma_j \vec{E}_0$ and $\vec{E}_0^\dagger \gamma_j \vec{E}_0$ into Eq. (4) and demanding both $\vec{\upsilon}_e$ and $\vec{E}_0$ to point towards the $\langle 111 \rangle$-direction, i.e. $\vec{\upsilon}_e(E) = \upsilon_e^{111}(E)\vec{E}_0$, yields

$$
\begin{aligned}
\vec{\upsilon}_e(E) &= \mathscr{A}(E) \sum_{j=1}^{4} \frac{n_j}{n} \frac{\gamma_j \vec{E}_0}{\sqrt{\vec{E}_0^\dagger \gamma_j \vec{E}_0}} \\
\vec{\upsilon}_e(E) &= \mathscr{A}(E) \left(\frac{n_1}{n} \sqrt{L}\, \vec{E}_0 + 3 \frac{n_2}{n} \sqrt{\frac{8}{9}T + \frac{1}{9}L}\, \vec{E}_0 \right) \\
\Rightarrow \upsilon_e^{111}(E) &= \mathscr{A}(E) \left(\frac{n_1}{n} \sqrt{L} + \left(1 - \frac{n_1}{n}\right) \sqrt{\frac{8}{9}T + \frac{1}{9}L} \right) \\
\Rightarrow \frac{n_1}{n} &= \frac{\frac{\upsilon_e^{111}(E)}{\mathscr{A}(E)} - \sqrt{\frac{8}{9}T + \frac{1}{9}L}}{\sqrt{L} - \sqrt{\frac{8}{9}T + \frac{1}{9}L}} .
\end{aligned}
\tag{8}
$$

The result from Eq. (8) is identified with Eq. (5) for the case $j = 1$, yielding

$$
\begin{aligned}
\mathscr{R}(E) &= \frac{\frac{n_1}{n} - \frac{n_e}{n}}{\frac{(\vec{E}_0^\dagger \gamma_1 \vec{E}_0)^{-1/2}}{\sum_{i=1}^{4} (\vec{E}_0^\dagger \gamma_i \vec{E}_0)^{-1/2}} - \frac{n_e}{n}} = \frac{\frac{\frac{\upsilon_e^{111}(E)}{\mathscr{A}(E)} - \sqrt{\frac{8}{9}T + \frac{1}{9}L}}{\sqrt{L} - \sqrt{\frac{8}{9}T + \frac{1}{9}L}} - \frac{1}{4}}{\frac{\frac{1}{\sqrt{L}}}{\frac{1}{\sqrt{L}} + 3\frac{1}{\sqrt{\frac{8}{9}T + \frac{1}{9}L}}} - \frac{1}{4}} \\
&= \underbrace{-\frac{4}{3} \frac{3\sqrt{L} + \sqrt{\frac{8}{9}T + \frac{1}{9}L}}{\left(\sqrt{L} - \sqrt{\frac{8}{9}T + \frac{1}{9}L}\right)^2}}_{= \Gamma_1} \frac{\upsilon_e^{111}(E)}{\mathscr{A}(E)} + \underbrace{\frac{1}{3} \frac{(\sqrt{L} + 3\sqrt{\frac{8}{9}T + \frac{1}{9}L})(3\sqrt{L} + \sqrt{\frac{8}{9}T + \frac{1}{9}L})}{\left(\sqrt{L} - \sqrt{\frac{8}{9}T + \frac{1}{9}L}\right)^2}}_{= \Gamma_2} .
\end{aligned}
\tag{9}
$$

Plugging in the values for $m_{e,T}^*$ and $m_{e,L}^*$ results in $\Gamma_1 = -1.182$ and $\Gamma_2 = 3.161$.

2.2 Silicon

In silicon, the conduction band minima lay along the three degenerate Δ-directions, i.e. $\langle 100 \rangle$, $\langle 010 \rangle$ and $\langle 001 \rangle$. The electrons populating the minima have effective masses between the transverse effective electron mass, $m_{e,T}^* = 0.19$, and the longitudinal effective electron mass, $m_{e,L}^* = 0.98$, with values given in units of the electron mass [8].

2.2.1 Determination of γ_j

The transformations of γ_0 to γ_j are similar to the ones presented for germanium. The only difference is that the local coordinate system $x'y'z'$ of the conduction band minima are chosen such that the initial y'-axis points towards one of the three equivalent Δ-directions. With $T = 1/m^*_{e,T}$, $L = 1/m^*_{e,L}$, $c = \cos(\varphi_{110})$ and $s = \sin(\varphi_{110})$, this yields

$$
\begin{aligned}
\gamma_1 &= R_1^{-1}\gamma_0 R_1 = R_z^{-1}(\varphi_{110})R_z^{-1}(\pi/4)\;\gamma_0\;R_z(\pi/4)\;R_z(\varphi_{110}) \\
&= \begin{bmatrix} c & -s & 0 \\ s & c & 0 \\ 0 & 0 & 1 \end{bmatrix}
\begin{bmatrix} \sqrt{\frac{1}{2}} & -\sqrt{\frac{1}{2}} & 0 \\ \sqrt{\frac{1}{2}} & \sqrt{\frac{1}{2}} & 0 \\ 0 & 0 & 1 \end{bmatrix}
\begin{bmatrix} T & 0 & 0 \\ 0 & L & 0 \\ 0 & 0 & T \end{bmatrix}
\begin{bmatrix} \sqrt{\frac{1}{2}} & \sqrt{\frac{1}{2}} & 0 \\ -\sqrt{\frac{1}{2}} & \sqrt{\frac{1}{2}} & 0 \\ 0 & 0 & 1 \end{bmatrix}
\begin{bmatrix} c & s & 0 \\ -s & c & 0 \\ 0 & 0 & 1 \end{bmatrix} \\
&= \begin{bmatrix} \frac{1}{2}T+\frac{1}{2}L+(T-L)\,cs & (-\frac{1}{2}T+\frac{1}{2}L)(c^2-s^2) & 0 \\ (-\frac{1}{2}T+\frac{1}{2}L)(c^2-s^2) & \frac{1}{2}T+\frac{1}{2}L+(L-T)\,cs & 0 \\ 0 & 0 & T \end{bmatrix}, \\
\gamma_2 &= R_2^{-1}\gamma_0 R_2 = R_z^{-1}(\varphi_{110})R_z^{-1}(-\pi/4)\;\gamma_0\;R_z(-\pi/4)\;R_z(\varphi_{110}) \\
&= \begin{bmatrix} c & -s & 0 \\ s & c & 0 \\ 0 & 0 & 1 \end{bmatrix}
\begin{bmatrix} \sqrt{\frac{1}{2}} & \sqrt{\frac{1}{2}} & 0 \\ -\sqrt{\frac{1}{2}} & \sqrt{\frac{1}{2}} & 0 \\ 0 & 0 & 1 \end{bmatrix}
\begin{bmatrix} T & 0 & 0 \\ 0 & L & 0 \\ 0 & 0 & T \end{bmatrix}
\begin{bmatrix} \sqrt{\frac{1}{2}} & -\sqrt{\frac{1}{2}} & 0 \\ \sqrt{\frac{1}{2}} & \sqrt{\frac{1}{2}} & 0 \\ 0 & 0 & 1 \end{bmatrix}
\begin{bmatrix} c & s & 0 \\ -s & c & 0 \\ 0 & 0 & 1 \end{bmatrix} \\
&= \begin{bmatrix} \frac{1}{2}T+\frac{1}{2}L+(L-T)\,cs & (\frac{1}{2}T-\frac{1}{2}L)(c^2-s^2) & 0 \\ (\frac{1}{2}T-\frac{1}{2}L)(c^2-s^2) & \frac{1}{2}T+\frac{1}{2}L+(T-L)\,cs & 0 \\ 0 & 0 & T \end{bmatrix}, \text{ and} \\
\gamma_3 &= R_3^{-1}\gamma_0 R_3 = R_z^{-1}(\varphi_{110})R_z^{-1}(\pi/4)\;R_{x'}^{-1}(\pi/2)\;\gamma_0\;R_{x'}(\pi/2)\;R_z(\pi/4)\;R_z(\varphi_{110}) \\
&= \begin{bmatrix} c & -s & 0 \\ s & c & 0 \\ 0 & 0 & 1 \end{bmatrix}
\begin{bmatrix} \sqrt{\frac{1}{2}} & -\sqrt{\frac{1}{2}} & 0 \\ \sqrt{\frac{1}{2}} & \sqrt{\frac{1}{2}} & 0 \\ 0 & 0 & 1 \end{bmatrix}
\begin{bmatrix} 1 & 0 & 0 \\ 0 & 0 & 1 \\ 0 & -1 & 0 \end{bmatrix}
\begin{bmatrix} T & 0 & 0 \\ 0 & L & 0 \\ 0 & 0 & T \end{bmatrix}
\begin{bmatrix} 1 & 0 & 0 \\ 0 & 0 & -1 \\ 0 & 1 & 0 \end{bmatrix} \cdot \\
&\quad \cdot \begin{bmatrix} \sqrt{\frac{1}{2}} & \sqrt{\frac{1}{2}} & 0 \\ -\sqrt{\frac{1}{2}} & \sqrt{\frac{1}{2}} & 0 \\ 0 & 0 & 1 \end{bmatrix}
\begin{bmatrix} c & s & 0 \\ -s & c & 0 \\ 0 & 0 & 1 \end{bmatrix}
= \begin{bmatrix} T & 0 & 0 \\ 0 & T & 0 \\ 0 & 0 & L \end{bmatrix}.
\end{aligned}
$$

2.2.2 Determination of $\mathscr{A}$

Choosing $\varphi_{110} = 0$, an electric field vector pointing along the $\langle 111\rangle$ axis can be expressed through $\vec{E}_0 = [\sqrt{2/3}, 0, \sqrt{1/3}]$. As in the case for germanium, this yields $\vec{E}_0^\dagger \gamma_j \vec{E}_0 = \frac{2}{3}T + \frac{1}{3}L$ for all three j. As all three minima are equally favoured, all Δ-directions contribute equally to the electron drift and are equally populated, i.e. $\frac{n_j}{n} = \frac{1}{3}$.

Therefore,

$$
\begin{aligned}
\vec{v}_e(E) &= \mathscr{A}(E)\sum_{j=1}^{3}\frac{n_j}{n}\frac{\gamma_j\vec{E}_0}{\sqrt{\vec{E}_0^\dagger\gamma_j\vec{E}_0}} = \mathscr{A}(E)\,\frac{1}{3}\frac{1}{\sqrt{\frac{2}{3}T+\frac{1}{3}L}}\sum_{j=1}^{3}\gamma_j\vec{E}_0\,.\\
&= \mathscr{A}(E)\,\frac{1}{3}\frac{1}{\sqrt{\frac{2}{3}T+\frac{1}{3}L}}\left(2T+L\right)\,\vec{E}_0 = \mathscr{A}(E)\sqrt{\frac{2}{3}T+\frac{1}{3}L}\,\vec{E}_0 \stackrel{!}{=} \upsilon_e^{111}(E)\,\vec{E}_0\\
&\Rightarrow \mathscr{A}(E) = \frac{\upsilon_e^{111}(E)}{\sqrt{\frac{2}{3}T+\frac{1}{3}L}} =: \frac{\upsilon_e^{111}(E)}{\Gamma_0}, \qquad (10)
\end{aligned}
$$

where $\Gamma_0 = \sqrt{\frac{2}{3}T+\frac{1}{3}L}$. Using $m^*_{e,T} = 0.19$ and $m^*_{e,L} = 0.98$ results in $\Gamma_0 = 1.962$.

2.2.3 Determination of $\mathscr{R}$

If an electric field along the $\langle 100\rangle$ axis is applied, one conduction band minimum is favoured over the others. With $\varphi_{110} = 0$, an electric field along the $\langle 100\rangle$ axis is given by $\vec{E}_0 = [\sqrt{1/2},\sqrt{1/2},0]$. Thus, the electrons in the minimum aligned with the electric field vector, $j = 1$, have the longitudinal effective mass, $\vec{E}_0^\dagger\gamma_1\vec{E}_0 = L$, while the other two, $j = 2,3$, have the transverse effective mass, $\vec{E}_0^\dagger\gamma_j\vec{E}_0 = T$. This also results in an unequal population of the minima with electrons, i.e. $\frac{n_1}{n} \neq \frac{n_2}{n} = \frac{n_3}{n}$. Inserting the values for $\gamma_j\vec{E}_0$ and $\vec{E}_0^\dagger\gamma_j\vec{E}_0$ into Eq. (4) and demanding both $\vec{\upsilon}_e$ and $\vec{E}_0$ to point towards the $\langle 100\rangle$-direction, i.e. $\vec{\upsilon}_e(E) = \upsilon_e^{100}(E)\vec{E}_0$, yields

$$
\begin{aligned}
\vec{v}_e(E) &= \mathscr{A}(E)\sum_{j=1}^{3}\frac{n_j}{n}\frac{\gamma_j\vec{E}_0}{\sqrt{\vec{E}_0^\dagger\gamma_j\vec{E}_0}} = \mathscr{A}(E)\left(\frac{n_1}{n}\sqrt{L}\,\vec{E}_0 + 2\frac{n_2}{n}\sqrt{T}\,\vec{E}_0\right)\\
\Rightarrow \upsilon_e^{100}(E) &= \mathscr{A}(E)\left(\frac{n_1}{n}\sqrt{L}+\left(1-\frac{n_1}{n}\right)\sqrt{T}\right)\\
\Rightarrow \frac{n_1}{n} &= \frac{\frac{\upsilon_e^{100}(E)}{\mathscr{A}(E)}-\sqrt{T}}{\sqrt{L}-\sqrt{T}}. \qquad (11)
\end{aligned}
$$

Plugging the result from Eq. (11) into Eq. (5) for the case $j = 1$ gives

$$
\begin{aligned}
\mathscr{R}(E) &= \frac{\frac{n_1}{n}-\frac{n_e}{n}}{\frac{(\vec{E}_0^\dagger\gamma_1\vec{E}_0)^{-1/2}}{\sum_{i=1}^{3}(\vec{E}_0^\dagger\gamma_i\vec{E}_0)^{-1/2}}-\frac{n_e}{n}} = \frac{\frac{\frac{\upsilon_e^{100}(E)}{\mathscr{A}(E)}-\sqrt{T}}{\sqrt{L}-\sqrt{T}}-\frac{1}{3}}{\frac{\frac{1}{\sqrt{L}}}{\frac{1}{\sqrt{L}}+2\frac{1}{\sqrt{T}}}-\frac{1}{3}}\\
&= \underbrace{-\frac{3}{2}\frac{\sqrt{T}+2\sqrt{L}}{\left(\sqrt{L}-\sqrt{T}\right)^2}}_{=\,\Gamma_1}\frac{\upsilon_e^{100}(E)}{\mathscr{A}(E)} + \underbrace{\frac{1}{2}\frac{(\sqrt{L}+2\sqrt{T})(\sqrt{T}+2\sqrt{L})}{\left(\sqrt{L}-\sqrt{T}\right)^2}}_{=\,\Gamma_2}.
\end{aligned}
$$

Plugging in the values for $m^*_{e,T}$ and $m^*_{e,L}$ results in $\Gamma_1 = -3.925$ and $\Gamma_2 = 7.325$.

3 Hole drift model as implemented in SolidStateDetectors.jl

Holes in germanium and silicon populate the valence band maximum at the Γ-point. Thus, in the absence of an electric field, the mean wave vector, $\vec{k}_0$, of all holes is expected to be 0. Holes have a slightly higher effective mass when drifting in $\langle 111 \rangle$-direction compared to all other directions. At the Γ-point, there are multiple degenerate $\langle 111 \rangle$-directions due to the multiplicity of L-points in the first Brillouin zone. Hence, not only one but multiple directions are equally favoured for the hole drift.

The presence of $\vec{E}$ changes the mean wave vector to $\vec{k}_0 \neq 0$, i.e. the $\vec{k}$-states are no longer equiprobable. The hole drift velocity, $\vec{v}_h$, is given by averaging the velocity contributions from each $\vec{k}$-state. The hole drift model described by B. Bruyneel *et al.* [9] considers only heavy holes in the valence band and suggests

$$\vec{v}_h(\vec{r},T) = \frac{\hbar}{a\pi^{3/2}\sqrt{2m^*_{hh}k_B T_{hh}}} \int_{\mathbb{R}^3} \mathrm{d}^3k \;\; \vec{v}(\vec{k}) f(\vec{k},\vec{k}_0(\vec{E}(\vec{r}))), \tag{12}$$

where $f(\vec{k},\vec{k}_0)$ denotes the wave vector distribution of heavy holes which can be approximated by a drifted Maxwellian distribution [10] with $\vec{k}_0$ pointing parallel to $\vec{E}$:

$$f(\vec{k},\vec{k}_0) = a \cdot \exp\left(-\frac{\hbar^2(\vec{k}-\vec{k}_0)^2}{2m^*_{hh}k_B T_{hh}}\right). \tag{13}$$

In both equations, a is a normalisation factor, k_B is the Boltzmann constant and T_{hh} is the temperature of the heavy holes.

The hole drift velocity, $\vec{v}(\vec{k})$, associated with a specific $\vec{k}$-state is defined by the band structure of the heavy holes, $E_h(\vec{k})$. In spherical coordinates, $\vec{k} = \vec{k}(k,\theta,\varphi)$, it is

$$\vec{v}(\vec{k}) = \frac{1}{\hbar}\vec{\nabla}_k E_h(\vec{k})|_{\vec{k}} \quad \text{with} \quad E_h(\vec{k}) = A\,\frac{\hbar^2 k^2}{2m_e}\,(1-q(\theta,\varphi))$$
$$\text{and} \quad q(\theta,\varphi) = \sqrt{b^2 + \frac{c^2}{4}\,(\sin(\theta)^4\sin(2\varphi)^2 + sin(2\theta)^2)} \tag{14}$$

$$\vec{\nabla}_k E_h(\vec{k}) = \frac{\partial E_h}{\partial k}\vec{e}_k + \frac{1}{k}\frac{\partial E_h}{\partial \theta}\vec{e}_\theta + \frac{1}{k\sin(\theta)}\frac{\partial E_h}{\partial \varphi}\vec{e}_\varphi = \frac{A\hbar^2 k}{m_e}(1-q(\theta,\varphi))\,\vec{e}_k \tag{15}$$
$$- \left[\frac{c^2 A\hbar^2 k}{8m_e q(\theta,\varphi)}\left(2\sin(\theta)^3\cos(\theta)\sin(2\varphi)^2 + \sin(4\theta)\right)\vec{e}_\theta + \sin(\theta)^3\sin(4\varphi)\,\vec{e}_\varphi\right]$$

where A, b, c are material-specific parameters, and $\vec{e}_k$, $\vec{e}_\theta$, $\vec{e}_\varphi$ are the unit vectors in the local spherical coordinate system. Using $\mathrm{d}^3k = k^2\sin(\theta)\mathrm{d}k\mathrm{d}\theta\mathrm{d}\varphi$, the integral over k in Eq. (12) can be solved analytically, leaving a two-dimensional integral over θ and φ.

When aligning the x-axis with the $\langle 100\rangle$ axis, the hole drift velocity in x-direction, υ_h^x, can be expressed using spherical coordinates $\vec{k}(k,\theta,\varphi)$ and $\vec{k}_0(k_0,\theta_0,\varphi_0)$, where the polar and azimuth angle θ_0 and φ_0 are aligned with $\vec{E}(E,\theta_0,\varphi_0)$:

$$\upsilon_h^x(\vec{k}_0) = \frac{\upsilon_h^{100}(k_0)}{n(k_0)} \int_0^{2\pi}\int_0^{\pi} X(\theta,\varphi)\,\exp(k_0^2(R^2-1))\,I_3(k_0R)\,\sin(\theta)\,\mathrm{d}\theta\mathrm{d}\varphi \tag{16}$$

with factors in the integral being

$$\begin{aligned}
X(\theta,\varphi) &= \frac{1}{k}\vec{\nabla}_k E_h(\vec{k})\cdot\vec{e}_x = \frac{A\hbar^2}{m_e}\,(1-q(\theta,\varphi))\cos(\varphi)\sin(\theta) \\
&\quad - \frac{c^2A\hbar^2}{8m_e q(\theta,\varphi)}\left(2\sin(\theta)^3\cos(\theta)\sin(2\varphi)^2+\sin(4\theta)\right)\cos(\varphi)\cos(\theta) \\
&\quad + \frac{c^2A\hbar^2}{8m_e q(\theta,\varphi)}\sin(\theta)^3\sin(4\varphi)\sin(\varphi) \\
R(\theta,\varphi,\theta_0,\varphi_0) &= \frac{\vec{k}}{k}\cdot\frac{\vec{k}_0}{k_0} = \sin(\theta_0)\sin(\theta)\cos(\varphi-\varphi_0)+\cos(\theta_0)\cos(\theta) \\
I_3(x) &= \int_0^{\infty} k^3\exp(-(k-x)^2)\mathrm{d}k = \frac{\sqrt{\pi}}{2}\left(x^2+\frac{1}{2}\right)(1+\mathrm{erf}(x))+\frac{1}{2}(x^2+1)\exp(-x^2).
\end{aligned} \tag{17}$$

The function $n(k_0)$ can be obtained by numerically evaluating the integral in Eq. (16) in $\langle 100\rangle$-direction, i.e. by setting $\theta_0=\pi/2$ and $\varphi_0=0$, for different k_0:

$$n(k_0) = \int_0^{2\pi}\int_0^{\pi} X(\theta,\varphi)\,\exp(k_0^2(R^2-1))\,I_3(k_0R)\,\sin(\theta)\mathrm{d}\theta\mathrm{d}\varphi$$

Using an approximation inspired by the warped band structure of the valence band [11] and defining the relative difference in radial velocity, $\Lambda(E)$, and the relative tangential velocity, $\Omega(E)$, as functions of the longitudinal hole-drift velocities along the $\langle 100\rangle$ and $\langle 110\rangle$ axes, υ_h^{100} and υ_h^{110}, and the transverse hole-drift velocity of the bisector between the two axes, $\upsilon_h^{\varphi}(\theta=\frac{\pi}{2},\varphi=\frac{\pi}{8})$:

$$\Lambda(E) = \frac{\upsilon_h^{100}(E)-\upsilon_h^{110}(E)}{\upsilon_h^{100}(E)} \qquad \Omega(E) = \frac{\upsilon_h^{\varphi}(\theta=\frac{\pi}{2},\varphi=\frac{\pi}{8})(E)}{\upsilon_h^{100}(E)} \tag{18}$$

allows to evaluate the three-dimensional integral in Eq. (12) and express $\vec{\upsilon}_h$ in spherical coordinates. The functions $\Lambda(k_0)$ and $\Omega(k_0)$ are obtained by numerically solving the integral in Eq. (16) for different k_0.

Along the $\langle 110 \rangle$-direction, i.e. $\theta_0 = \pi/2$ and $\varphi_0 = \pi/4$, the contributions from drift along x- and y-directions are equal, i.e. $\upsilon_h^x(k_0) = \upsilon_h^y(k_0)$. Thus, the drift velocity along the $\langle 110 \rangle$-direction, $\vec{\upsilon}_h^{110}(k_0) = [\upsilon_h^x(k_0), \upsilon_h^x(k_0), 0]$, has the absolute value $\upsilon_h^{110}(k_0) = \sqrt{2}\upsilon_h^x(k_0)$. In Eq. (16), $\upsilon_h^x(k_0) = \upsilon_h^{110}(k_0)/\sqrt{2}$ yields

$$\frac{\upsilon_h^{110}(k_0)\, n(k_0)}{\upsilon_h^{100}(k_0)\sqrt{2}} = \int_0^{2\pi}\int_0^{\pi} X(\theta,\varphi)\, \exp(k_0^2(R^2-1))\, I_3(k_0R)\sin(\theta)\mathrm{d}\theta\mathrm{d}\varphi$$

$$\Lambda(k_0) = 1 - \frac{\upsilon_h^{110}(k_0)}{\upsilon_h^{100}(k_0)} = 1 - \frac{\sqrt{2}}{n(k_0)}\int_0^{2\pi}\int_0^{\pi} X(\theta,\varphi)\, \exp(k_0^2(R^2-1))\, I_3(k_0R)\sin(\theta)\mathrm{d}\theta\mathrm{d}\varphi$$

The computation of $\Omega(k_0)$ is more complex. It is obtained by setting $\theta_0 = \pi/2$ and $\varphi_0 = \pi/8$, and calculating $\Omega(k_0) = (-\sin(\pi/8)\upsilon_h^x(k_0) + \cos(\pi/8)\upsilon_h^y(k_0))/\upsilon_h^{100}(k_0)$:

$$\frac{\upsilon_h^x(k_0)}{\upsilon_h^{100}(k_0)} = \frac{1}{n(k_0)}\int_0^{2\pi}\int_0^{\pi} X(\theta,\varphi)\, \exp(k_0^2(R^2-1))\, I_3(k_0R)\sin(\theta)\mathrm{d}\theta\mathrm{d}\varphi$$

and $\upsilon_h^y(k_0)/\upsilon_h^{100}(k_0)$ is calculated accordingly by replacing $X(\theta,\varphi)$ with $Y(\theta,\varphi)$, i.e. replacing $\vec{e}_x$ with $\vec{e}_y$ in Eq. (17). The functions $\Lambda(k_0)$ and $\Omega(k_0)$ define the hole the drift velocity, using a good approximation which takes a similar form as $\vec{\nabla}_k E_h(\vec{k})$ in Eq. (15). The radial, polar and azimuth components of $\vec{\upsilon}_h$ result in

$$\upsilon_h^r(\vec{r}) = \upsilon_h^{100}(E(\vec{r}))\,[1-\Lambda(k_0)(\sin(\theta_0)^4\sin(2\varphi_0)^2 + \sin(2\theta_0)^2] \tag{19}$$
$$\upsilon_h^\theta(\vec{r}) = \upsilon_h^{100}(E(\vec{r}))\,\Omega(k_0)\,[2\sin(\theta_0)^3\cos(\theta_0)\sin(2\varphi_0)^2 + \sin(4\theta_0)] \tag{20}$$
$$\upsilon_h^\varphi(\vec{r}) = \upsilon_h^{100}(E(\vec{r}))\,\Omega(k_0)\,\sin(\theta_0)^3\sin(4\varphi_0). \tag{21}$$

This approximation is valid for $k_0 < 3$, which corresponds to the electric field strengths expected in solid state detectors. The quantity k_0 needs to be linked to a physical observable, as for example the relative velocity $\upsilon_{\mathrm{rel}} = \upsilon_h^{111}/\upsilon_h^{100}$. For fast computation, an analytical function should be determined for this.

In contrast to the original publication from Bruyneel *et al.* [9], the analytical expressions for Λ and Ω will not be functions of k_0 but directly depend on υ_{rel}. Evaluating Eq. (19) along the $\langle 111 \rangle$ direction results in

$$\upsilon_h^{111} = \upsilon_h^{100}\left[1 - \frac{4}{3}\Lambda(k_0)\right] \quad \Rightarrow \Lambda(\upsilon_{\mathrm{rel}}) = \frac{3}{4}(1-\upsilon_{\mathrm{rel}}) \tag{22}$$

which is independent of any material-specific parameters present in Eq. (14).

The expression for $\Omega(\upsilon_{\mathrm{rel}})$ is determined by calculating $\Omega(k_0)$ and $\upsilon_{\mathrm{rel}}(k_0)$ for a set of k_0 and fitting the resulting points to a fourth-order polynomial in orders of $(1-\upsilon_{\mathrm{rel}})$[1].

[1] This ensures $\Omega(\upsilon_{\mathrm{rel}} = 1) = 0$, i.e. no anisotropy in the isotropic case $\upsilon_h^{100} = \upsilon_h^{111} \Leftrightarrow \upsilon_{\mathrm{rel}} = 1$.

3.1 Germanium

The material-specific parameters needed for Eq. (14) are $A = 13.35$, $b = 0.6367$ and $c = 0.9820$ [9]. As the computation of the integral in Eq. (12) is time consuming, the approximations in Eqs. (19) to (21) are used for simulations with SolidStateDetectors.jl. The function $\Omega(\upsilon_{\text{rel}})$ is computed for a set of k_0 and fitted to a fourth-order polynomial in the region of interest, $0.3 \leq k_0 \leq 1.5$, see Fig. 3a:

$$\begin{aligned}\Omega(\upsilon_{\text{rel}}) = &-0.29711 \cdot (1-\upsilon_{\text{rel}}) \ -1.12082 \cdot (1-\upsilon_{\text{rel}})^2 \\ &+3.83929 \cdot (1-\upsilon_{\text{rel}})^3 - 4.80825 \cdot (1-\upsilon_{\text{rel}})^4\end{aligned} \tag{23}$$

3.2 Silicon

In silicon, the material-specific parameters used in Eq. (14) are $A = -4.0$, $b = 0.275$ and $c = 1.025$ [8]. Like for germanium, the function $\Omega(\upsilon_{\text{rel}})$ is approximated by a fourth-order polynomial in the region of interest, $0.3 \leq k_0 \leq 1.5$, see Fig. **??**a:

$$\begin{aligned}\Omega(\upsilon_{\text{rel}}) = &-0.30565 \cdot (1-\upsilon_{\text{rel}}) \ -1.19650 \cdot (1-\upsilon_{\text{rel}})^2 \\ &+4.69001 \cdot (1-\upsilon_{\text{rel}})^3 - 7.00635 \cdot (1-\upsilon_{\text{rel}})^4\end{aligned} \tag{24}$$

References

[1] D.M. Caughey and R.E. Thomas, Proc. IEEE **55**, 2192 (1967).

[2] L. Mihailescu *et al.*, Nucl. Instr. and Meth. A **447**, 350 (2000).

[3] G. Ottaviani *et al.*, IEEE Trans. Nucl. Sci. **22**, 192 (1975).

[4] B. Bruyneel *et al.*, Nucl. Instr. and Meth. A **569**, 774 (2006).

[5] R. Barrie and R.R. Burgess, Can. J. Phys. **40**, 1056 (1962).

[6] H.G. Reik and H. Risken, Phys. Rev. **126**, 1737 (1962).

[7] M.I. Nathan, Phys. Rev. **130**, 2201 (1963).

[8] R.N. Dexter *et al.*, Phys. Rev. **104**, 637 (1956).

[9] B. Bruyneel *et al.*, Nucl. Instr. and Meth. A **569**, 764 (2006).

[10] H. Nakagawa and S. Zukotynski, Can. J. Phys. **57**, 1233 (1979).

[11] L. Reggiani, *Hot-Electron Transport in Semiconductors*, 1st edition, (Springer-Verlag, Berlin Heidelberg, 1985), pp. 57–58.

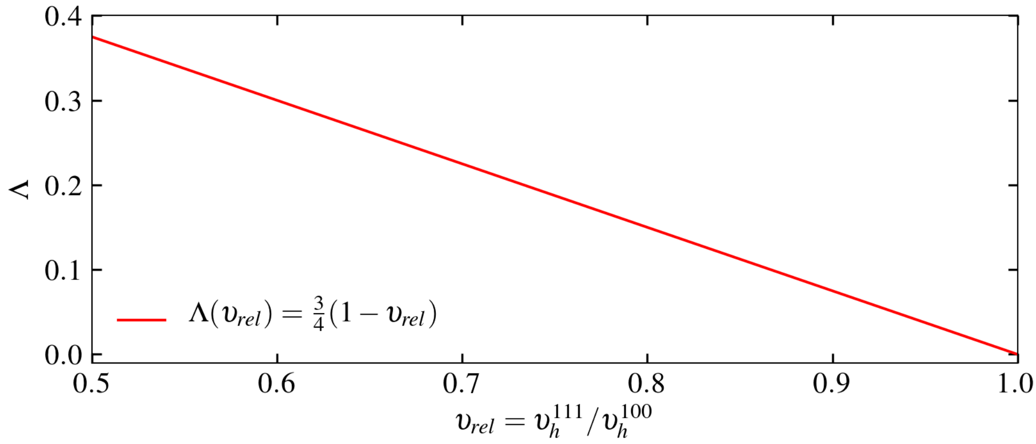

Figure 2: Analytical expression for $\Lambda(\upsilon_{\mathrm{rel}})$ for both germanium and silicon.

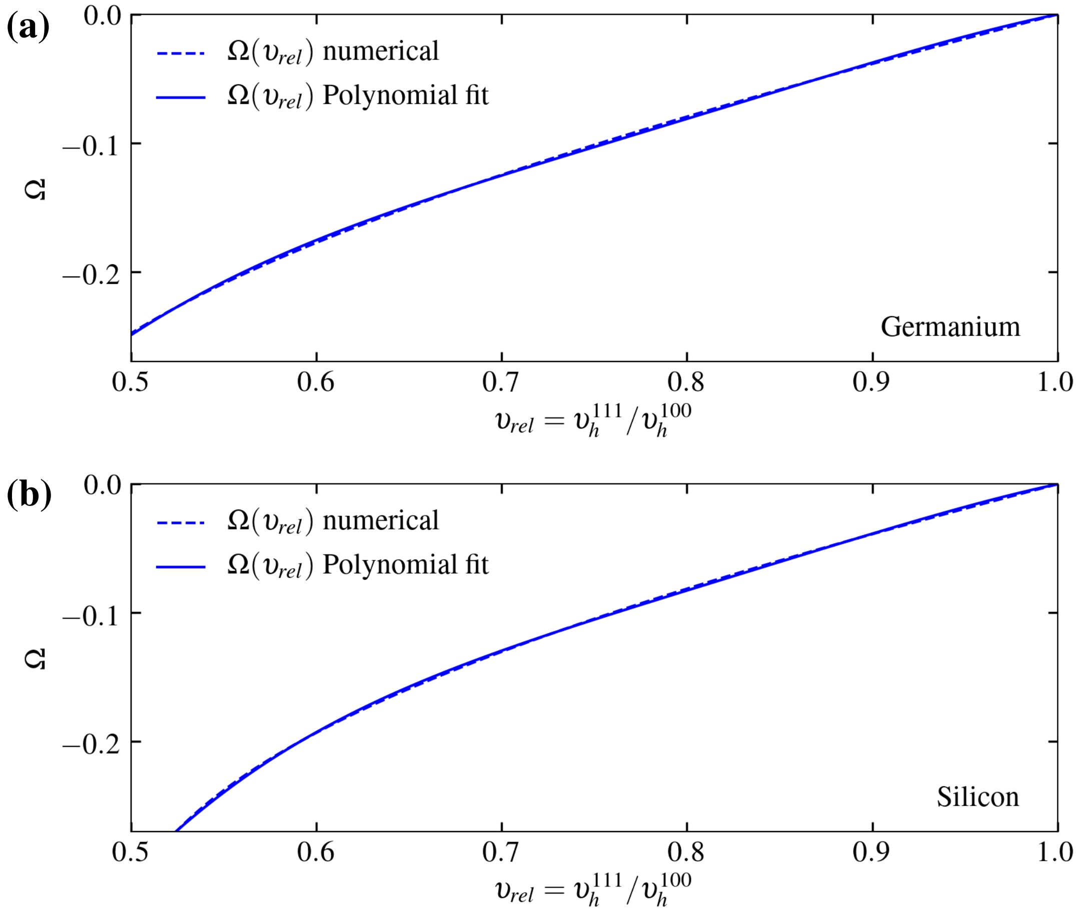

Figure 3: Calculated values for $\Omega(k_0)$ in (a) germanium and (b) silicon and corresponding fits to a fourth-order polynomial, see Eqs. (23) and (24). The values for $\Omega(k_0)$ and $\upsilon_{\mathrm{rel}}(k_0)$ were calculated for k_0 from 0 to 3 in steps of 0.01 and are connected by dashed lines. The fits are shown by solid lines.